Environmental Science & Technology

pubs.acs.org/est

Article

Photo-oxidation of Aromatic Hydrocarbons Produces Low-Volatility Organic Compounds

Mingyi Wang, Dexian Chen, Mao Xiao, Qing Ye, Dominik Stolzenburg, Victoria Hofbauer, Penglin Ye, Alexander L. Vogel, Roy L. Mauldin, III, Antonio Amorim, Andrea Baccarini, Bernhard Baumgartner, Sophia Brilke, Lubna Dada, António Dias, Jonathan Duplissy, Henning Finkenzeller, Olga Garmash, Xu-Cheng He, Christopher R. Hoyle, Changhyuk Kim, Alexander Kvashnin, Katrianne Lehtipalo, Lukas Fischer, Ugo Molteni, Tuukka Petäjä, Veronika Pospisilova, Lauriane L. J. Quéléver, Matti Rissanen, Mario Simon, Christian Tauber, António Tomé, Andrea C. Wagner, Lena Weitz, Rainer Volkamer, Paul M. Winkler, Jasper Kirkby, Douglas R. Worsnop, Markku Kulmala, Urs Baltensperger, Josef Dommen, Imad El-Haddad, and Neil M. Donahue*

Cite This: https://dx.doi.org/10.1021/acs.est.0c02100

Read Online

ACCESS | Metrics & More | Article Recommendations | Supporting Information

ABSTRACT: To better understand the role of aromatic hydrocarbons in new-particle formation, we measured the particle-phase abundance and volatility of oxidation products following the reaction of aromatic hydrocarbons with OH radicals. For this we used thermal desorption in an iodide-adduct Time-of-Flight Chemical-Ionization Mass Spectrometer equipped with a Filter Inlet for Gases and AEROsols (FIGAERO-ToF-CIMS). The particle-phase volatility measurements confirm that oxidation products of toluene and naphthalene can contribute to the initial growth of newly formed particles. Toluene-derived (C_7) oxidation products have a similar volatility distribution to that of α-pinene-derived (C_{10}) oxidation products, while naphthalene-derived (C_{10}) oxidation products are much less volatile than those from toluene or α-pinene; they are thus stronger contributors to growth. Rapid progression through multiple generations of oxidation is more pronounced in toluene and naphthalene than in α-pinene, resulting in more oxidation but also favoring functional groups with much lower volatility per added oxygen atom, such as hydroxyl and carboxylic groups instead of hydroperoxide groups. Under conditions typical of polluted urban settings, naphthalene may well contribute to nucleation and the growth of the smallest particles, whereas the more abundant alkyl benzenes may overtake naphthalene once the particles have grown beyond the point where the Kelvin effect strongly influences the condensation driving force.

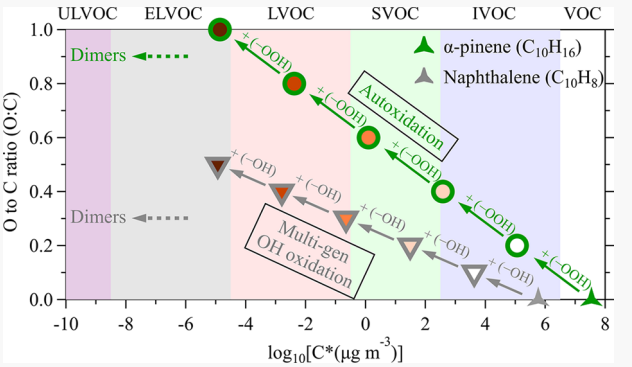

INTRODUCTION

Organic condensation from the gas phase to the particle phase contributes to particle growth and causes secondary organic aerosol (SOA) formation.[1] SOA in turn may comprise well over half of the total fine-particle mass in the lower atmosphere, contributing to and possibly dominating health effects include more than 4 million premature deaths per year.[2,3] However, to what extent organic condensation affects the initial growth of nucleated particles remains in doubt, and the mechanism forming "condensable" organic vapors is even less certain.[4] The growth rate of freshly nucleated particles is crucial to their survival,[5] which in turn governs the connection between particle nucleation and aerosol−cloud interactions, one of the most uncertain elements of the climate system.[6]

Recent results from the "Cosmics Leaving OUtdoor Droplets" (CLOUD) experiment show that organic vapors emitted by trees can produce abundant aerosol particles through nucleation of ultralow volatility organic compounds (ULVOCs) even when there is no sulfuric acid.[7] Tröstl et al.,[1] Lehtipalo et al.,[8] and Stolzenburg et al.[9] have constrained the role of pure biogenic organic vapors in the initial growth of nucleated particles via laboratory experiments free from inorganic acids and bases or nitrogen oxides (NO_x). Combined experimental data and model simulations show that biogenic organic vapors driving initial

Received: April 4, 2020
Revised: June 2, 2020
Accepted: June 9, 2020
Published: June 9, 2020

growth up to ~2 nm are extremely low-volatility organic compounds (ELVOCs). As particles grow and the Kelvin effect diminishes, subsequent growth is taken over by more abundant low-volatility organic compounds (LVOCs) with slightly higher volatility.[10]

Ozonolysis of terpenes, followed by peroxy-radical autoxidation via a succession of internal H atom transfer reactions, produces ULVOCs and ELVOCs within a few seconds after the initial attack by ozone.[11] This drives new-particle formation in regions dominated by biogenic emissions.[12] However, these processes can be suppressed substantially in polluted airmasses, where nitrogen oxides (NO_x) can perturb peroxy-radical chemistry and suppress ULVOC and ELVOC formation.[13] Further, even under optimal conditions, those compounds comprise only <5% of the terpene oxidation products.[14] Although first-generation auto-oxidation plays a major role, the (large) balance of "traditional" product vapors cannot be neglected; those vapors will undergo further oxidation, which has been shown to increase yields of SOA[15] and also to form more ELVOCs via subsequent autoxidation.[16]

Pollution contains much more than NO_x. In the urban atmosphere, aromatic hydrocarbons can account for up to 60% of the total VOCs.[17,18] Among them, small monocyclic aromatics are mostly emitted from anthropogenic sources, such as fossil-fuel combustion and solvent evaporation, with toluene being one of the most abundant species.[17,18] Polycyclic aromatic hydrocarbons mainly come from incomplete combustion such as heavy-duty diesel vehicles, biomass burning, and meat cooking;[19−21] formation of naphthalene is often favored among PAHs during these combustion processes.[20] Aromatic hydrocarbons are believed to play a critical role in the formation of both tropospheric ozone and secondary organic aerosols (SOA).[22−25] Laboratory studies have also reported highly oxygenated product formation from OH-triggered oxidation of aromatic hydrocarbons, highlighting their potential contribution to nucleation and initial particle growth in the anthropogenic environment.[26,27]

Despite the significance of aromatic systems to the urban atmosphere, the volatility profile of oxidation products from aromatic precursors has yet to be established. The contribution of aromatic-derived oxidation products to urban new-particle formation has so far remained ambiguous. Here, we extend previous CLOUD experiments on biogenic organic vapors to add toluene and naphthalene as examples of anthropogenic organic vapors, comparing the formation pathways of oxidized organics as well as their behaviors on contributing to the growth of newly formed particles in the urban environment.

MATERIALS AND METHODS

We conducted experiments involving aromatic precursors under typical urban conditions in the "Cosmics Leaving OUtdoor Droplets" (CLOUD) chamber. The CLOUD facility was constructed to measure nucleation and growth rates of inorganic and organic vapors under highly controlled, ultraclean conditions. The 26.1 m^3 stainless steel chamber is kept scrupulously clean, with background contaminants (H_2SO_4, organics, amines) < 10^5 cm^{-3}. It can be exposed to ultraviolet (UV) light via a fiber-optic system to generate OH radicals uniformly via ozone photolysis, initiating subsequent photochemical reactions. In addition, the Xe arc lights with UVA at 385 nm from a set of 400 W LED lights are augmented to photolyze NO_2 to NO. The chamber temperature can be controlled from 183 to 373 K,[28] and relative humidity (RH) from <0.5% to 101%, enabling experiments over a wide range of tropospheric conditions.

Experiment Conditions. Results presented here are from the CLOUD-11 campaign in Fall 2016. To simulate urban environments, we fixed the temperature at 20 °C, relative humidity at 60%, ozone concentration at ~40 ppbv, NH_3 concentration at ~500 pptv, SO_2 concentration at ~2 ppbv, and NO_2 concentration at ~1−2 ppbv. We conducted experiments with different aromatic precursor concentrations spanning urban conditions −8 ppbv and 40 ppbv for toluene and 2 ppbv and 15 ppbv for naphthalene. We formed OH radicals via ozone photolysis and the subsequent reaction of $O(^1D)$ with water vapor.

Chemical Ionization Mass Spectrometer. We measured the gas-phase and particle-phase composition as well as particle-phase volatility of oxidation products via thermal desorption using an iodide-adduct Time-of-Flight Chemical Ionization Mass Spectrometer equipped with a Filter Inlet for Gases and AEROsols (FIGAERO-ToF-CIMS). Iodide-adduct chemical ionization is well suited for measuring a suite of oxygenated organics with minimal fragmentation.[29] The FIGAERO is a manifold inlet for the CIMS with two operating modes.[30] In the first mode, gases are directly sampled into a turbulent flow ion−molecule reactor while particles are concurrently collected on a PTFE filter via a separate dedicated port. In the second mode, the filter is automatically moved into a pure N_2 gas stream flowing into the ion−molecule reactor while the N_2 is heated to evaporate the particles via temperature-programmed desorption. Analytes are then chemically ionized and extracted into a long ToF-MS, achieving sensitivities below 10^6 cm^{-3} on a 1 min average with very high mass resolution (up to 14 000).[31] This technique enhances our ability to explore the partitioning between the gas and particle phases driving the aerosol behavior. In addition, during CLOUD-11, H_2SO_4 and oxidized organic vapor concentrations were routinely measured with a nitrate-ion based Chemical Ionization Atmospheric Pressure interface Time-of-Flight mass spectrometer (nitrate-CI-APi-ToF).[7] Calibration and corrections of sulfuric acid are similar to our previous work.[32]

Particle Size Distribution. Particle size distributions were measured by several sizing instruments optimized for different size ranges. Particles in the size range between 1.8−8 nm were measured by the so-called DMA-train,[9] and the corresponding growth-rate calculations were performed with the appearance time method, which is effective in chamber experiments where a clear front of a growing particle population can be identified during most nucleation and growth events. Larger particles between 5−65 nm were measured with a scanning mobility particle sizer (TSI nano-SMPS, model 3982).

Volatility Measurements. Organic compounds with different vapor pressures have distinct and reproducible thermograms during thermal desorption, and the maximum desorption temperature (T_{max}) correlates with the vaporization enthalpy and thus is a function of the vapor pressure. We calibrated the thermal-desorption volatility measurements using a suite of standards with known vapor pressures.[30,33] Briefly, we dissolved a set of organic acids in isopropanol at low concentrations and manually deposited them on the FIGAERO filter with a microliter syringe. We then held the mixture of acids at room temperature for 1 min to allow the solvent to evaporate before following the same thermal-desorption protocol used for chamber experiments. We then established a thermal-desorption volatility calibration curve by correlating $1/T_{max}$ (1/K) with the

https://dx.doi.org/10.1021/acs.est.0c02100
Environ. Sci. Technol. XXXX, XXX, XXX−XXX

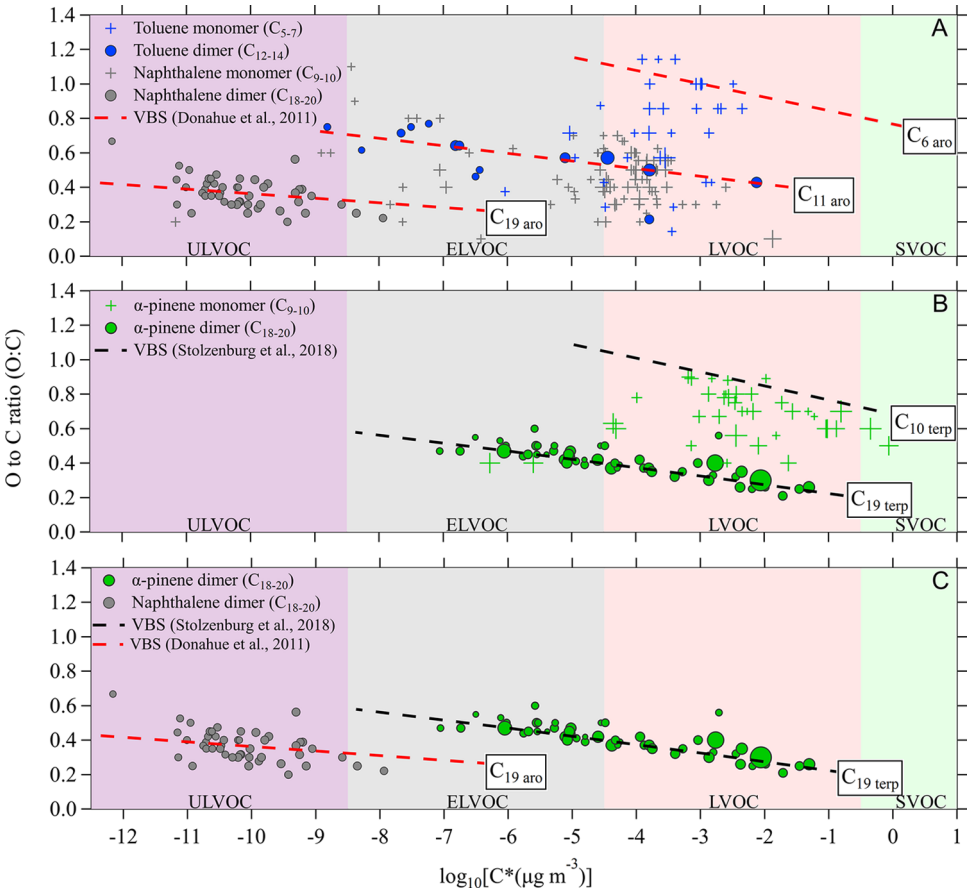

Figure 1. Directly measured particle-phase oxidation products plotted on a two-dimensional VBS. The background colors indicate the saturation concentration (C^*) range of ultralow volatility (ULVOCs, purple), extremely low volatility (ELVOCs, gray), low volatility (LVOCs, pink), and semivolatile (SVOCs, green) organic compounds. (A) Monomers (crosses) and dimers (dots) from toluene (blue symbols) and naphthalene (gray symbols) photo-oxidation with NO_x present. The volatility distribution can be represented by carbon numbers isopleths (red dashed lines) derived from the original volatility basis set (VBS) parameterization.[35] (B) Monomers (green crosses) and dimers (green dots) from α-pinene ozonolysis with NO_x present observed in CLOUD 11 experiments as well as carbon numbers isopleths (black dashed lines) calculated using a revised VBS parameterization to reflect the −OOH functionality formed via autoxidation.[9] (C) Direct comparison of aromatic-derived dimers and α-pinene-derived dimers. Both are C_{20} but the aromatics are much less volatile than α-pinene-derived dimers. Symbol sizes are proportional to the particle-phase signals.

subcooled liquid vapor pressure of each calibrant (Figure S1 of the Supporting Information, SI). One potential source of uncertainty is that dimers may decompose to monomers when heated, appearing as doublet-peaks in the thermogram.[34] However, in this study, as dimer formation is suppressed by NO_x, thermal decomposition of dimers did not affect the T_{max} of monomers.

RESULTS AND DISCUSSION

Direct Measurement of Particle-Phase Volatility. In the experiments described above we directly measured the volatility of particle-phase products formed from photo-oxidation of representative aromatic precursors (toluene and naphthalene) via their thermal-desorption profile using an I^- FIGAERO−CIMS (see Materials and Methods). In Figure 1, we display the results in the two-dimensional volatility basis set (2D-VBS),[35] with volatility (saturation concentration, C^*, in $\mu g\ m^{-3}$) on the x-axis and the oxygenation (oxygen to carbon ratio, O:C) on the y-axis. We choose C^* and O:C as two complementary coordinates because they explicitly track properties that we can observe in experiments and in the atmosphere, and that we need to know to accurately model organic aerosol behavior.

In Figure 1A, we show monomers (crosses) and dimers (dots) derived from photo-oxidation of toluene (blue symbols) and naphthalene (gray symbols) with NO_x present. Almost all of the naphthalene-derived dimers appear in the ULVOC range,[36] but the toluene-derived dimers span the LVOC and ELVOC ranges. The measured monomers mostly appear in the LVOC range, with a minority of the naphthalene-derived monomers being ELVOCs. Red dashed lines are carbon numbers isopleths (C_6, C_{11}, and C_{19}); these are derived from the original 2D-VBS volatility parameterization, developed before the role of autoxidation in atmospheric chemistry was appreciated,[37] which assumed that a 50−50 mixture of −OH and =O functionalities dominated the oxidized organics.[35] These contours coincide well with our measured volatilities from aromatic precursors. Toluene-derived monomers and naphthalene-derived dimers fall along the C_6 and C_{19} isopleths, respectively, and toluene-derived dimers and naphthalene-derived monomers overlap along the C_{11} isopleths. Measured monomers are slightly more spread than dimers, potentially due to thermal decomposition or dehydration.

Similar to our aromatic oxidation experiments, in Figure 1B, we present monomers (green crosses) and dimers (green dots) from α-pinene ozonolysis in the presence of NO_x. The carbon

https://dx.doi.org/10.1021/acs.est.0c02100
Environ. Sci. Technol. XXXX, XXX, XXX−XXX

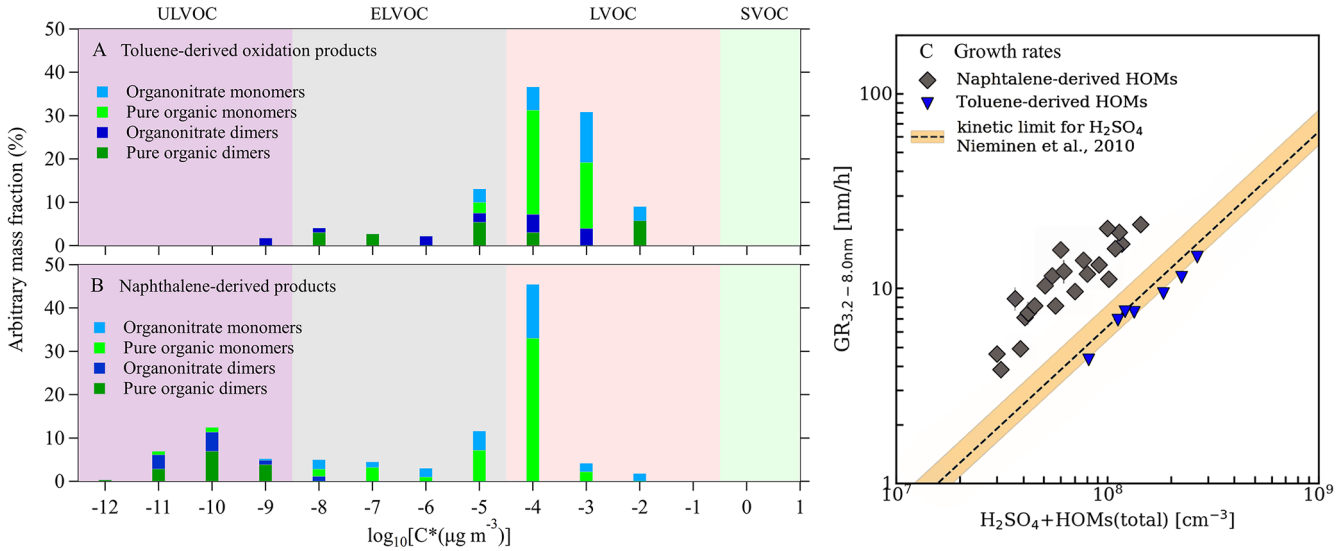

Figure 2. Directly measured volatility distributions of particle-phase products formed during toluene (A) and naphthalene (B) photo-oxidation with NO_x present. Products are binned with the measured relative mass concentration in percent. The measured oxidation products are divided into organonitrate monomers (light blue), pure organic monomers (light green), organonitrate dimers (navy blue), and pure organic dimers (dark green). (C) Growth rates measured with DMA train vs the sum of sulfuric acid and HOM concentrations. Sulfuric acid kinetic limit is taken from Nieminen et al.[53]

number isopleths (C_{10} and C_{19}, black dashed lines) are calculated using a revised VBS parameterization to reflect the contribution of autoxidation and subsequent −OOH functionality formation to initial particle growth.[9] The measured dimers align with the C_{19} isopleth with great fidelity, though monomers are systematically but only slightly less volatile than the C_{10} isopleth. In this case, NO terminates the nascent peroxy radicals, suppresses autoxidation, and thus reduces the product oxygen numbers. As a result, the overall product volatility distribution is shifted toward the volatile end of the distribution compared to NO_x-free products (the oxygens on the $-NO_2$ moiety are not counted in O:C). Nevertheless, the products remain well described by the modified C* vs O:C isopleths, with much higher volatility than the "traditional" VBS.

Compared with the α-pinene-derived oxidation products (C_{10}), toluene-derived products reach a similar volatility and O:C range with a C_7 backbone. More interestingly, naphthalene-derived oxidation products are much less volatile than α-pinene-derived products, although both start with a C_{10} backbone. The general volatility difference between dimers from these two precursors is ∼5 orders of magnitude, as illustrated in Figures 1C and S2. Aromatic oxidation appears to use oxygen atoms much more efficiently to form low-volatility products, consistent with the observation that bulk aromatic aerosols have a larger volume fraction remaining (VFR) after heating than biogenic aerosols.[38]

In Figure S3, we show the measured volatilities of aromatic- and α-pinene-derived oxidation products versus corresponding volatilities estimated using the VBS parameterizations in Donahue et al.[35] and Stolzenburg et al.,[9] respectively. Here, we choose organic compounds with six or more oxygen atoms to minimize the uncertainty of thermal decomposition in the FIGAERO. A good correlation (r^2 of 0.77) verifies the consistency between direct FIGAERO volatility measurements and VBS parameterizations.

Correlation between Volatility and Growth Rate. Because the volatility of photo-oxidation products can vary by more than 10 orders of magnitude, it is convenient to simplify consideration of gas-particle partitioning by grouping compounds together within the VBS. In Figure 2A and 2B we show the binned volatility distribution of all organic particle-phase compounds observed with our FIGAERO−CIMS for the two representative aromatic hydrocarbons. The volatility of toluene-derived oxidation products (Figure 2A) ranges from 10^{-9} to 10^{-2} $\mu g\ m^{-3}$ with one mode at 10^{-4} and the other at 10^{-8} $\mu g\ m^{-3}$. Naphthalene oxidation products are even less volatile (Figure 2B), with saturation concentrations ranging from 10^{-12} to 10^{-2} $\mu g\ m^{-3}$. We divide the measured oxidation products into four groups: organonitrate monomers (light blue), pure organic monomers (light green), organonitrate dimers (navy blue), and pure organic dimers (dark green). For both of the monomers and dimers, organonitrates tend to be more volatile than non-nitrate products. This is again consistent with the NO_x effect on monoterpene oxidation and can also be explained either by the termination of nascent peroxy radicals or by reduced product reactivity with OH radicals and thus less secondary oxidation.

The measured volatility distributions are consistent with the 3−8 nm growth-rate measurements, where in Figure 2C we compare observed growth rates with gas-phase oxidation products measured with a nitrate-CI-APi-TOF.[13] With most of the products in the LVOC range, toluene-derived oxidation products are somewhat less efficient than H_2SO_4 at driving growth. Naphthalene oxidation, on the other hand, produces a large amount of ULVOCs and ELVOCs, which are relatively more efficient at driving growth. The consistency between volatility and growth-rate measurements makes sense since all the species that can be measured in the particle phase must contribute to the particle growth, thus their volatilities can be taken as the criteria of growing particles and be used by VBS microphysical growth models.

The relative contribution of different precursors to new-particle formation depends on the volatility distribution of the products as well as the relative concentrations of the precursors. In polluted urban atmospheres, the concentration of aromatic hydrocarbons will exceed that of monoterpenes to be the

https://dx.doi.org/10.1021/acs.est.0c02100
Environ. Sci. Technol. XXXX, XXX, XXX−XXX

dominant VOC precursors. Further, NO_x will substantially suppress the formation of monoterpene-derived ELVOCs, making the role of aromatic-derived oxidation products even more important. It is thus essential to add the volatility distribution of aromatic-derived oxidation products into particle-growth models and to assess the growth rates observed in urban areas.

Influence of Functionality on Volatility. Volatility is affected by both the molar weight and polarity of a molecule. Therefore, molecular structure and functionality matter. As a hydrocarbon chain gets larger, the increase in number of electrons increases the temporary dipoles causing stronger van der Waals' forces and thus reducing the volatility. According to the SIMPOL model,[39] each carbon atom lowers log C^* by 0.44. However, toluene has fewer carbon atoms than α-pinene, yet forms oxidation products with a comparable volatility distribution (see Figure 1). This is not due directly to aromaticity; each aromatic ring only lowers log C^* by 0.68. Even more notably, the 4 to 5 decades general difference between naphthalene-derived and α-pinene-derived oxidation products cannot be explained by different structures of their carbon backbones. This leaves functionality as the driving factor; the identity of the added functional groups plays a major role in volatility. Addition of one oxygen-containing functional group, in general, has a greater effect on volatility than a one-carbon increase in the size of the carbon skeleton, but the exact nature of the functional group is very important. Polar functional groups promote dipole−dipole interactions and thus will result in a larger decrease in volatility (e.g., each aldehyde group reduces log C^* by 1.35, and ketone group by 0.94). Functional groups that enable hydrogen bonding between molecules result in an even larger decrease in volatility (e.g., each hydroxyl group reduces log C^* by 2.23, hydroperoxide group by 2.48 (1.24 per oxygen), and carboxylic acid group by 3.58 (1.79 per oxygen)).[39]

We investigate the influence of oxygen-containing functional groups on volatility of aromatic- and α-pinene-derived oxidation products by performing a parameterization using FIGAERO volatility data. This parameterization is based on a simple, three-parameter group-contribution expression:

$$\log_{10} C^*_{300} = (n^0_C - n_C)b_C - n_O b_O \quad (1)$$

where C^*_{300} (at 300 K) is calculated from SIMPOL or directly measured by FIGAERO; $n^0_C = 25$ is the carbon number n_C with $C^O = 1\ \mu g\ m^{-3}$ for pure hydrocarbons; $b_C = 0.48$ is the average effect of each added carbon on $\log_{10} C^*$; b_O indicates the average effect of each added oxygen on $\log_{10} C^*$.[35] Note that a nitrate group ($-ONO_2$) typically reduces vapor pressure by about 2.5 orders of magnitude, so we replace any $-ONO_2$ group by $-OH$ for simplicity.

Here, instead of using this parameterization to calculate volatility, we fit the parameter b_O using volatility measured with FIGAERO thermal desorption. We performed the parameterization for products from α-pinene ozonolysis, toluene photo-oxidation, and naphthalene photo-oxidation, all with NO_x (green, blue, and gray symbols in Figure 1, respectively).

The fitted b_O value for α-pinene-derived oxidation products with NO_x present is 0.91. This is consistent with hydroperoxide, ketone, and aldehyde functionalities (roughly 1 decade per oxygen) proposed in Tröstl et al.[1] To the extent that these simple group-contribution values can be extrapolated to multifunctional compounds, this appears to be general within the confines of this data set; it certainly applies at the low-O:C limit, and it is reasonable for bifunctional compounds (e.g., diacids[40]). Many of the low-volatility particle-phase products from monoterpene oxidation may thus be first-generation autoxidation products containing multiple −OOH functional groups.

The fitted b_O values for toluene-derived and naphthalene-derived oxidation products, however, are 1.55 and 1.72, respectively, suggesting more hydroxyl or carboxylic acid functionality in aromatic-derived products. Oxygen-containing groups are very likely the key to the systematic volatility difference between aromatic and monoterpene oxidation systems, so we investigate the chemical mechanism in the next section to further understand the formation of these functional groups in aromatic oxidation systems.

Formation of Oxidation Products of Aromatic Hydrocarbons. In this section, we use toluene as the example to consider the chemical mechanism of aromatic oxidation. With this proposed mechanism, we are able to address the volatility distributions arising from aromatics and evaluate the contribution of aromatic-derived oxidation products to new-particle formation.

The detailed chemical mechanism of toluene oxidation in the atmosphere remains uncertain. Wu et al.[41] suggested that over 75% bicyclic peroxy radicals (BPRs) are formed after the first OH oxidation of toluene based on a modified MCM mechanism. Wang et al.,[42] combining quantum calculations and flow-tube experiments, proposed that unimolecular H-migration followed by O_2-addition, a so-called autoxidation step, can take place in BPRs, which are important intermediates of the OH-initiated oxidation of alkyl benzenes.[43] Alternatively, Ji et al.[44] reported that cresols are much more stable than their corresponding peroxy radicals,[45] and, for the most favorable OH (ortho) addition, the pathway of H abstraction by O_2 to form the cresol is dominant and O_2 addition to form the peroxy radical is negligible. Other comprehensive studies[46,47] identified ring-retaining products from cresol oxidation and quantified both the yields of dihydroxy toluene and trihydroxy toluene being ∼0.7, which supported the results from Ji et al.[44]

These seemingly disparate findings may not be contradictory, since product formation pathways and their yields depend strongly on experimental conditions. In the case of toluene oxidation, the concentrations of OH radicals and O_2 control the relative importance of OH oxidation and autoxidation, respectively. Wang et al.[42] worked with [OH] of $(2.4–53) \times 10^4$ cm^{-3} in their experiments, which is one to 2 orders of magnitude lower than in ambient conditions. The predominance of BPRs observed in their experiments could be due to suppressed OH oxidation. However, in Ji's experiments,[44] the concentration of O_2 was 10^{15} cm^{-3}, roughly 5000 times lower than in the atmospheric boundary layer ($[O_2] = 5 \times 10^{18}$ cm^{-3}), which could substantially suppress the formation of peroxy radicals.

In the CLOUD experiments, we set the experimental conditions as close as possible to ambient conditions in order to acquire insights into the mechanisms that are atmospherically relevant. We used [OH] of $\sim 10^6$ cm^{-3} and the [NO_x] of ∼15 ppbv for the experiments in this study. Also, the iodide reagent ion in our FIGAERO is sensitive to a wide range of species, enabling us to observe oxygenated organics with oxygen numbers down to one or two with good fidelity.[48] Under these conditions, we observed products from both categories. In Figure 3 we show a mass defect plot of monomers from toluene

https://dx.doi.org/10.1021/acs.est.0c02100
Environ. Sci. Technol. XXXX, XXX, XXX−XXX

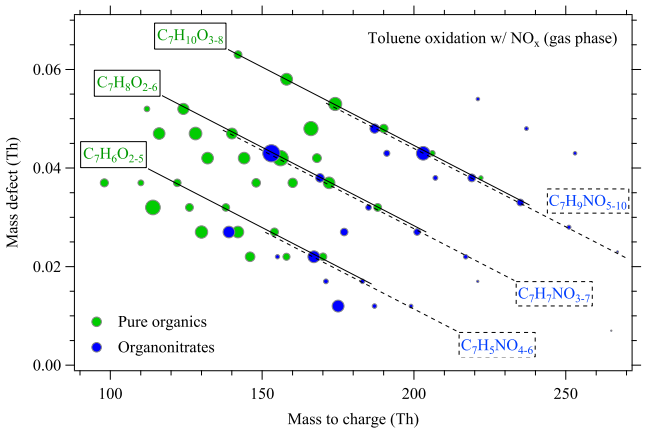

Figure 3. Mass defect plot showing products from toluene oxidation measured in the gas phase. The *x*-axis is the exact mass of oxidation products and *y*-axis is the mass defect. The color of circles denotes the type of products, and their size is proportional to the logarithm of the count rate. Each straight line represents a group of compounds with the same number of carbon, hydrogen, and nitrogen atoms, but a different number of oxygen atoms.

oxidation measured in the gas phase. The *x*-axis is the exact mass of the products and the *y*-axis is the mass defect. Each straight line represents a homologous sequence of compounds with the same number of carbon, hydrogen, and nitrogen atoms, but a different number of oxygen atoms. Notably, there are two main categories of products: $C_7H_8O_{2-6}$, which likely preserves the aromaticity, and $C_7H_{10}O_{4-8}$, which breaks the aromatic ring. These aromatic ring-retaining and aromatic ring-opening products are associated with organonitrates, $C_7H_7NO_{3-7}$ and $C_7H_9NO_{5-10}$, respectively, via the termination of the corresponding peroxy radicals by NO.

The detailed toluene oxidation mechanism is instructive (see Figure 4). Briefly, the rate of OH addition to an aromatic ring is proportional to the electrophilic nature of the substituents around the ring. Being electrophilic, the added OH groups in turn facilitate further addition reactions by increasing the electron density on the ring through a resonance donating effect and thus activating the aromatic ring. Following the ring-retaining pathway for toluene, OH radical addition to the aromatic ring can occur multiple times to form cresol, dihydroxy-, trihydroxy-, and even multi−OH substituted-toluene (i.e., $C_7H_8O_{2-6}$,). The fact that we did not observe a significant amount of cresol could be due to its relatively slow production and fast consumption, which yields a low steady-state vapor concentration. This is consistent with the large signal we observed for $C_7H_7NO_3$, most likely hydroxy nitrotoluene, formed from the reaction of methyl phenoxy radicals with NO_2 or the reaction of cresol with NO_3 radicals.[47]

Along the ring-opening pathway, peroxy radical production is followed by formation of bicyclic peroxides (i.e., $C_7H_{10}O_{4-8}$), which generates oxidation products with oxygen numbers of 8 or more. A succession of unimolecular H-migration reactions followed by O_2 addition (so-called autoxidation) can take place rapidly in bicyclic peroxy radicals (BPRs), which are important intermediates of the OH-initiated oxidation of aromatic compounds, possibly leading to the formation of highly oxygenated organic molecules (HOMs). However, with NO_x present in the chamber, peroxy-radical autoxidation is substantially suppressed, and we observed low HOM concentrations. Further, we also observed various decomposition products (C_5 and C_6) attributable to the bicyclic intermediate

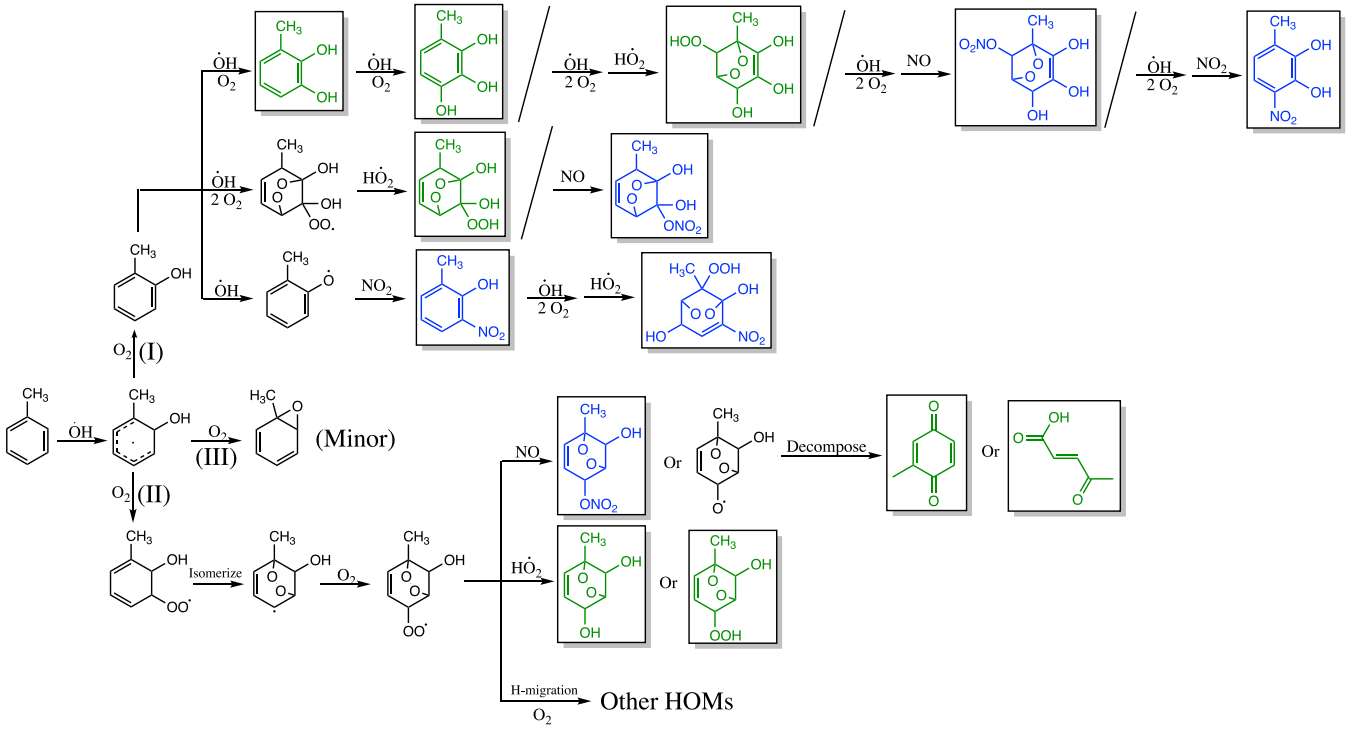

Figure 4. Gas-phase chemical mechanism for toluene photo-oxidation with NO_x present. The reaction starts with OH addition to the aromatic ring, resulting in oxidized radicals. Closed-shell products will be formed after radicals undergo various termination pathways. Products outlined are detected by the iodide-adduct CIMS. Non-nitrate products and organonitrate products are marked with green and blue, respectively. (Adapted from Schwantes et al.[47].)

https://dx.doi.org/10.1021/acs.est.0c02100
Environ. Sci. Technol. XXXX, XXX, XXX−XXX

pathway. Although we distinguish the OH oxidation pathway from the autoxidation pathway, product formation in reality does not follow only one pathway. OH oxidation and autoxidation both can occur; it is their branching ratio under different conditions that matters.

Our purpose here is not to comprehensively define the detailed mechanism, but rather to demonstrate that aromatics are qualitatively different from monoterpenes in terms of the chemical mechanisms of photo-oxidation leading to new-particle formation and particle growth. From the proposed mechanism and from our FIGAERO observations, we conclude that rapid progression through multiple generations of OH oxidation is more pronounced in toluene and naphthalene than that in α-pinene, resulting in not only more oxidation but crucially also functional groups with much lower volatility per added oxygen atom, such as hydroxyl and carboxylic acids. For example, our proposed $C_7H_xO_{5-7}$ products from toluene contain up to 4 hydroxyl groups, while $C_{10}H_xO_{5-7}$, from α-pinene proposed in Tröstl et al.,[1] only contain at most 1 hydroxyl group. Since hydroxyl groups have a much stronger effect per oxygen on volatility (stronger by about 1 decade per oxygen than −OOH), the larger number of hydroxyl groups accounts for the 4 to 5 decades difference in volatility between aromatic- and α-pinene-derived oxidation products we observe in Figure 1.

These findings are consistent with findings for bulk SOA formation from monoterpenes and aromatics.[49] Specifically, with monoterpenes (especially for ozonolysis), SOA mass yields can be reasonably described by first-generation products and a relatively stable product distribution following the initial ozonolysis. For toluene photo-oxidation, however, models of SOA formation in chambers must consider multiple generations of OH reaction because the products become progressively more reactive with OH as the generation number increases. To account for these differences, two different 2D-VBS representations of SOA formation and aging have been developed for chemical transport models.[50] Our findings confirm the differences. The volatility parameter $b_O \approx 1.6$ we derive for aromatic oxidation is consistent with the original 2D-VBS parameterization representing aging and oxygenation of organic products principally with an equal mixture of =O and −OH functional groups (and −C(O)OH). This is a "traditional aging" scenario. However, the volatility parameter $b_O \approx 0.9$ we derive for α-pinene oxidation is consistent with the modified parameterizations more recently employed to represent prompt formation of multiple −OOH functional groups. This is an "autoxidation" scenario.

It is important to note that these scenarios are not mutually exclusive. As we discussed, autoxidation does occur in the aromatic systems, and most of the first-generation monoterpene products are not HOMs that have undergone autoxidation. All of these (mostly gas-phase) products will almost certainly undergo further oxidation in the atmosphere, often on short time scales,[51] and some of these second and later generation products will also undergo autoxidation, as previous CLOUD experiments have shown for the first-generation monoterpene product pinanediol.[16,52]

Photo-oxidation of aromatic compounds (toluene and naphthalene) efficiently produces low-volatility products that participate in new-particle formation and growth under conditions typical of polluted urban settings. Here we have measured the composition of newly formed particles with a FIGAERO−CIMS and directly constrained the volatility distribution of the oxidation products that drive new-particle formation and growth. We find that oxidation of toluene and naphthalene by OH radicals makes efficient use of added oxygen to form low-volatility products, with much larger reductions in volatility per added oxygen atom than corresponding α-pinene systems. This is consistent with known differences in the oxidation mechanisms of aromatics and monoterpenes. Particle formation and growth in urban airmasses may thus be strongly influenced by aromatic precursors.

■ ASSOCIATED CONTENT

Supporting Information

The Supporting Information is available free of charge at https://pubs.acs.org/doi/10.1021/acs.est.0c02100.

Figure S1, Correlation of inverse maximum desorption temperature ($1/T_{max}$) and the saturation concentration ($\log C^*$); Figure S2, example of thermograms; and Figure S3, measured and predicted volatility (PDF)

■ AUTHOR INFORMATION

Corresponding Author

Neil M. Donahue − *Center for Atmospheric Particle Studies, Department of Chemistry, Department of Chemical Engineering, and Department of Engineering and Public Policy, Carnegie Mellon University, Pittsburgh, Pennsylvania 15213, United States;* orcid.org/0000-0003-3054-2364; Email: nmd@andrew.cmu.edu

Authors

Mingyi Wang − *Center for Atmospheric Particle Studies and Department of Chemistry, Carnegie Mellon University, Pittsburgh, Pennsylvania 15213, United States;* orcid.org/0000-0001-5782-2513

Dexian Chen − *Center for Atmospheric Particle Studies and Department of Chemical Engineering, Carnegie Mellon University, Pittsburgh, Pennsylvania 15213, United States*

Mao Xiao − *Laboratory of Atmospheric Chemistry, Paul Scherrer Institute, 5232 Villigen, Switzerland*

Qing Ye − *Center for Atmospheric Particle Studies and Department of Chemistry, Carnegie Mellon University, Pittsburgh, Pennsylvania 15213, United States;* orcid.org/0000-0003-3797-8988

Dominik Stolzenburg − *Faculty of Physics, University of Vienna, 1090 Vienna, Austria*

Victoria Hofbauer − *Center for Atmospheric Particle Studies and Department of Chemistry, Carnegie Mellon University, Pittsburgh, Pennsylvania 15213, United States*

Penglin Ye − *Aerodyne Research, Incorporated, Billerica, Massachusetts 01821, United States*

Alexander L. Vogel − *Institute for Atmospheric and Environmental Sciences, Goethe University Frankfurt, 60438 Frankfurt am Main, Germany;* orcid.org/0000-0002-1293-6370

Roy L. Mauldin, III − *Department of Oceanic and Atmospheric Science, University of Colorado Boulder, Boulder, Colorado 80309, United States; Center for Atmospheric Particle Studies and Department of Chemistry, Carnegie Mellon University, Pittsburgh, Pennsylvania 15213, United States*

Antonio Amorim − *CENTRA and FCUL, University of Lisbon, 1749-016 Lisbon, Portugal*

Andrea Baccarini − *Laboratory of Atmospheric Chemistry, Paul Scherrer Institute, 5232 Villigen, Switzerland*

https://dx.doi.org/10.1021/acs.est.0c02100
Environ. Sci. Technol. XXXX, XXX, XXX−XXX

Bernhard Baumgartner − *Faculty of Physics, University of Vienna, 1090 Vienna, Austria*
Sophia Brilke − *Faculty of Physics, University of Vienna, 1090 Vienna, Austria*
Lubna Dada − *Institute for Atmospheric and Earth System Research (INAR), University of Helsinki, 00014 Helsinki, Finland*
António Dias − *CENTRA and FCUL, University of Lisbon, 1749-016 Lisbon, Portugal*
Jonathan Duplissy − *Institute for Atmospheric and Earth System Research (INAR) and Helsinki Institute of Physics, University of Helsinki, 00014 Helsinki, Finland;* orcid.org/0000-0001-8819-0264
Henning Finkenzeller − *Department of Chemistry & CIRES, University of Colorado Boulder, Boulder, Colorado 80309, United States*
Olga Garmash − *Institute for Atmospheric and Earth System Research (INAR), University of Helsinki, 00014 Helsinki, Finland*
Xu-Cheng He − *Institute for Atmospheric and Earth System Research (INAR), University of Helsinki, 00014 Helsinki, Finland;* orcid.org/0000-0002-7416-306X
Christopher R. Hoyle − *Laboratory of Atmospheric Chemistry, Paul Scherrer Institute, 5232 Villigen, Switzerland; Institute for Atmospheric and Climate Science, ETH Zurich, 8092 Zurich, Switzerland*
Changhyuk Kim − *Division of Chemistry and Chemical Engineering, California Institute of Technology, Pasadena, California 91125, United States; Department of Environmental Engineering, Pusan National University, Busan 46241, Republic of Korea*
Alexander Kvashnin − *Lebedev Physical Institute, 119991 Moscow, Russia*
Katrianne Lehtipalo − *Institute for Atmospheric and Earth System Research (INAR), University of Helsinki, 00014 Helsinki, Finland; Finnish meteorological Institute, 00560 Helsinki, Finland*
Lukas Fischer − *Institute for Ion Physics and Applied Physics, University of Innsbruck, 6020 Innsbruck, Austria;* orcid.org/0000-0002-3141-9088
Ugo Molteni − *Laboratory of Atmospheric Chemistry, Paul Scherrer Institute, 5232 Villigen, Switzerland*
Tuukka Petäjä − *Institute for Atmospheric and Earth System Research (INAR), University of Helsinki, 00014 Helsinki, Finland*
Veronika Pospisilova − *Laboratory of Atmospheric Chemistry, Paul Scherrer Institute, 5232 Villigen, Switzerland*
Lauriane L. J. Quéléver − *Institute for Atmospheric and Earth System Research (INAR), University of Helsinki, 00014 Helsinki, Finland*
Matti Rissanen − *Aerosol Physics Laboratory, Physics Unit, Tampere University, Tampere 33100, Finland;* orcid.org/0000-0003-0463-8098
Mario Simon − *Institute for Atmospheric and Environmental Sciences, Goethe University Frankfurt, 60438 Frankfurt am Main, Germany*
Christian Tauber − *Faculty of Physics, University of Vienna, 1090 Vienna, Austria;* orcid.org/0000-0003-1453-1067
António Tomé − *IDL−University of Beira Interior, Covilhã 6201-001, Portugal*
Andrea C. Wagner − *Institute for Atmospheric and Environmental Sciences, Goethe University Frankfurt, 60438 Frankfurt am Main, Germany; Department of Chemistry & CIRES, University of Colorado Boulder, Boulder, Colorado 80309, United States*
Lena Weitz − *Institute for Atmospheric and Environmental Sciences, Goethe University Frankfurt, 60438 Frankfurt am Main, Germany*
Rainer Volkamer − *Department of Chemistry & CIRES, University of Colorado Boulder, Boulder, Colorado 80309, United States*
Paul M. Winkler − *Faculty of Physics, University of Vienna, 1090 Vienna, Austria*
Jasper Kirkby − *CERN, 1211 Geneva, Switzerland; Institute for Atmospheric and Environmental Sciences, Goethe University Frankfurt, 60438 Frankfurt am Main, Germany*
Douglas R. Worsnop − *Institute for Atmospheric and Earth System Research (INAR), University of Helsinki, 00014 Helsinki, Finland; Aerodyne Research, Incorporated, Billerica, Massachusetts 01821, United States*
Markku Kulmala − *Institute for Atmospheric and Earth System Research (INAR) and Helsinki Institute of Physics, University of Helsinki, 00014 Helsinki, Finland; Joint International Research Laboratory of Atmospheric and Earth System Sciences, Nanjing University, Nanjing 210044, P. R. China; Aerosol and Haze Laboratory, Beijing Advanced Innovation Center for Soft Matter Science and Engineering, Beijing University of Chemical Technology, Beijing 100029, P. R. China*
Urs Baltensperger − *Laboratory of Atmospheric Chemistry, Paul Scherrer Institute, 5232 Villigen, Switzerland*
Josef Dommen − *Laboratory of Atmospheric Chemistry, Paul Scherrer Institute, 5232 Villigen, Switzerland;* orcid.org/0000-0002-0006-0009
Imad El-Haddad − *Laboratory of Atmospheric Chemistry, Paul Scherrer Institute, 5232 Villigen, Switzerland;* orcid.org/0000-0002-2461-7238

Complete contact information is available at: https://pubs.acs.org/10.1021/acs.est.0c02100

Author Contributions

M.W., D.C., M.X., J.K., D.R.W., U.B., J.Do., I.E.-H., and N.M.D. designed the research; M.W., D.C., M.X., Q.Y., D.S., V.H., P.Y., A.L.V., R.L.M., A.A., A.B., B.B., S.B., L.D., A.D., J.Du., H.F., O.G., X.H., C.R.H., C.K., A.K., K.L., F.L., U.M., T.P., V.P., L.L. J.Q., M.R., M.S., C.T., A.T., A.C.W., L.W., J.K., J.Do., and I.E.-H. performed the research; M.W., M.X., D.S., and N.M.D. contributed new reagents/analytic tools; M.W., M.X., D.S., P.Y., and M.S. analyzed the data; and M.W., D.C., M.X., A.L.V., U.M., J.K., U.B., J.Do., I.E.-H., and N.M.D. wrote the paper.

Notes

The authors declare no competing financial interest.

■ ACKNOWLEDGMENTS

We thank the European Organization for Nuclear Research (CERN) for supporting CLOUD with important technical and financial resources and for providing a particle beam from the CERN Proton Synchrotron. This research has received funding from the U.S. National Science Foundation under grants AGS-1447056, AGS-1439551, AGS-1649147, AGS-1602086, and AGS-1801897; the German Federal Ministry of Education and Research (No. 01LK1601A); ERC-Consolidator Grant NANO-DYNAMITE 616075; Horizon 2020 Marie Skłodowska-Curie Grant 656994 ("Nano-CAVa"); ERC Advanced "ATM-GP" grant No. 227463; the Presidium of the Russian Academy of Sciences, the Program "High energy physics and neutrino

astrophysics" 2015; the Swiss National Science Foundation Projects 200020_152907, 20FI20_159851, 200021_169090, 200020_172602, and 20FI20_172622. The FIGAERO−CIMS was supported by an MRI grant for the U.S. NSF AGS-1531284 as well as the Wallace Research Foundation. O.G. thanks the Doctoral Programme in Atmospheric Sciences at the University of Helsinki for financial support.

REFERENCES

(1) Tröstl, J.; Chuang, W. K.; Gordon, H.; Heinritzi, M.; Yan, C.; Molteni, U.; Ahlm, L.; Frege, C.; Bianchi, F.; Wagner, R.; Simon, M.; Lehtipalo, K.; Williamson, C.; Craven, J. S.; Duplissy, J.; Adamov, A.; Almeida, J.; Bernhammer, A. K.; Breitenlechner, M.; Brilke, S.; Dias, A.; Ehrhart, S.; Flagan, R. C.; Franchin, A.; Fuchs, C.; Guida, R.; Gysel, M.; Hansel, A.; Hoyle, C. R.; Jokinen, T.; Junninen, H.; Kangasluoma, J.; Keskinen, H.; Kim, J.; Krapf, M.; Kürten, A.; Laaksonen, A.; Lawler, M.; Leiminger, M.; Mathot, S.; Möhler, O.; Nieminen, T.; Onnela, A.; Petäjä, T.; Piel, F. M.; Miettinen, P.; Rissanen, M. P.; Rondo, L.; Sarnela, N.; Schobesberger, S.; Sengupta, K.; Sipilä, M.; Smith, J. N.; Steiner, G.; Tomè, A.; Virtanen, A.; Wagner, A. C.; Weingartner, E.; Wimmer, D.; Winkler, P. M.; Ye, P.; Carslaw, K. S.; Curtius, J.; Dommen, J.; Kirkby, J.; Kulmala, M.; Riipinen, I.; Worsnop, D. R.; Donahue, N. M.; Baltensperger, U. The Role of Low-Volatility Organic Compounds in Initial Particle Growth in the Atmosphere. *Nature* **2016**, *533* (7604), 527−531.

(2) Apte, J. S.; Marshall, J. D.; Cohen, A. J.; Brauer, M. Addressing Global Mortality from Ambient PM2.5. *Environ. Sci. Technol.* **2015**, *49* (13), 8057−8066.

(3) Lelieveld, J.; Evans, J. S.; Fnais, M.; Giannadaki, D.; Pozzer, A. The Contribution of Outdoor Air Pollution Sources to Premature Mortality on a Global Scale. *Nature* **2015**, *525* (7569), 367−371.

(4) Riipinen, I.; Yli-Juuti, T.; Pierce, J. R.; Petaja, T.; Worsnop, D. R.; Kulmala, M.; Donahue, N. M.; Petäjä, T.; Worsnop, D. R.; Kulmala, M.; et al. The Contribution of Organics to Atmospheric Nanoparticle Growth. *Nat. Geosci.* **2012**, *5* (7), 453−458.

(5) Anttila, T.; Kerminen, V.-M. M.; Lehtinen, K. E. J. J. Parameterizing the Formation Rate of New Particles: The Effect of Nuclei Self-Coagulation. *J. Aerosol Sci.* **2010**, *41* (7), 621−636.

(6) Solomon, S.; Manning, M.; Marquis, M.; Qin, D.; others. Climate Change 2007-the Physical Science Basis: Working Group I Contribution to the Fourth Assessment Report of the IPCC; Cambridge University Press, 2007; Vol. *4*.

(7) Kirkby, J.; Duplissy, J.; Sengupta, K.; Frege, C.; Gordon, H.; Williamson, C.; Heinritzi, M.; Simon, M.; Yan, C.; Almeida, J.; et al. Ion-Induced Nucleation of Pure Biogenic Particles. *Nature* **2016**, *533* (7604), 521−526.

(8) Lehtipalo, K.; Yan, C.; Dada, L.; Bianchi, F.; Xiao, M.; Wagner, R.; Stolzenburg, D.; Ahonen, L. R.; Amorim, A.; Baccarini, A.; Bauer, P. S.; Baumgartner, B.; Bergen, A.; Bernhammer, A.-K.; Breitenlechner, M.; Brilke, S.; Buchholz, A.; Mazon, S. B.; Chen, D.; Chen, X.; Dias, A.; Dommen, J.; Draper, D. C.; Duplissy, J.; Ehn, M.; Finkenzeller, H.; Fischer, L.; Frege, C.; Fuchs, C.; Garmash, O.; Gordon, H.; Hakala, J.; He, X.; Heikkinen, L.; Heinritzi, M.; Helm, J. C.; Hofbauer, V.; Hoyle, C. R.; Jokinen, T.; Kangasluoma, J.; Kerminen, V.-M.; Kim, C.; Kirkby, J.; Kontkanen, J.; Kürten, A.; Lawler, M. J.; Mai, H.; Mathot, S.; Mauldin, R. L.; Molteni, U.; Nichman, L.; Nie, W.; Nieminen, T.; Ojdanic, A.; Onnela, A.; Passananti, M.; Petäjä, T.; Piel, F.; Pospisilova, V.; Quéléver, L. L. J.; Rissanen, M. P.; Rose, C.; Sarnela, N.; Schallhart, S.; Schuchmann, S.; Sengupta, K.; Simon, M.; Sipilä, M.; Tauber, C.; Tomé, A.; Tröstl, J.; Väisänen, O.; Vogel, A. L.; Volkamer, R.; Wagner, A. C.; Wang, M.; Weitz, L.; Wimmer, D.; Ye, P.; Ylisirniö, A.; Zha, Q.; Carslaw, K. S.; Curtius, J.; Donahue, N. M.; Flagan, R. C.; Hansel, A.; Riipinen, I.; Virtanen, A.; Winkler, P. M.; Baltensperger, U.; Kulmala, M.; Worsnop, D. R. Multicomponent New Particle Formation from Sulfuric Acid, Ammonia, and Biogenic Vapors. *Sci. Adv.* **2018**, *4* (12), No. eaau5363.

(9) Stolzenburg, D.; Fischer, L.; Vogel, A. L.; Heinritzi, M.; Schervish, M.; Simon, M.; Wagner, A. C.; Dada, L.; Ahonen, L. R.; Amorim, A.; Baccarini, A.; Bauer, P. S.; Baumgartner, B.; Bergen, A.; Bianchi, F.; Breitenlechner, M.; Brilke, S.; Buenrostro Mazon, S.; Chen, D.; Dias, A.; Draper, D. C.; Duplissy, J.; El Haddad, I.; Finkenzeller, H.; Frege, C.; Fuchs, C.; Garmash, O.; Gordon, H.; He, X.; Helm, J.; Hofbauer, V.; Hoyle, C. R.; Kim, C.; Kirkby, J.; Kontkanen, J.; Kürten, A.; Lampilahti, J.; Lawler, M.; Lehtipalo, K.; Leiminger, M.; Mai, H.; Mathot, S.; Mentler, B.; Molteni, U.; Nie, W.; Nieminen, T.; Nowak, J. B.; Ojdanic, A.; Onnela, A.; Passananti, M.; Petäjä, T.; Quéléver, L. L. J.; Rissanen, M. P.; Sarnela, N.; Schallhart, S.; Tauber, C.; Tomé, A.; Wagner, R.; Wang, M.; Weitz, L.; Wimmer, D.; Xiao, M.; Yan, C.; Ye, P.; Zha, Q.; Baltensperger, U.; Curtius, J.; Dommen, J.; Flagan, R. C.; Kulmala, M.; Smith, J. N.; Worsnop, D. R.; Hansel, A.; Donahue, N. M.; Winkler, P. M. Rapid Growth of Organic Aerosol Nanoparticles over a Wide Tropospheric Temperature Range. *Proc. Natl. Acad. Sci. U. S. A.* **2018**, *115* (37), 9122−9127.

(10) Donahue, N. M.; Ortega, I. K.; Chuang, W.; Riipinen, I.; Riccobono, F.; Schobesberger, S.; Dommen, J.; Baltensperger, U.; Kulmala, M.; Worsnop, D. R.; Vehkamaki, H. How Do Organic Vapors Contribute to New-Particle Formation? *Faraday Discuss.* **2013**, *165*, 91−104.

(11) Jokinen, T.; Sipila, M.; Richters, S.; Kerminen, V. M.; Paasonen, P.; Stratmann, F.; Worsnop, D.; Kulmala, M.; Ehn, M.; Herrmann, H.; Berndt, T. Rapid Autoxidation Forms Highly Oxidized RO2 Radicals in the Atmosphere. *Angew. Chem., Int. Ed.* **2014**, *53*, 14596−14600.

(12) Ehn, M.; Thornton, J. A.; Kleist, E.; Sipila, M.; Junninen, H.; Pullinen, I.; Springer, M.; Rubach, F.; Tillmann, R.; Lee, B.; Lopez-Hilfiker, F.; Andres, S.; Acir, I. H.; Rissanen, M.; Jokinen, T.; Schobesberger, S.; Kangasluoma, J.; Kontkanen, J.; Nieminen, T.; Kurten, T.; Nielsen, L. B.; Jorgensen, S.; Kjaergaard, H. G.; Canagaratna, M.; Maso, M. D.; Berndt, T.; Petaja, T.; Wahner, A.; Kerminen, V. M.; Kulmala, M.; Worsnop, D. R.; Wildt, J.; Mentel, T. F.; Dal Maso, M.; Berndt, T.; Petaja, T.; Wahner, A.; Kerminen, V. M.; Kulmala, M.; Worsnop, D. R.; Wildt, J.; Mentel, T. F. A Large Source of Low-Volatility Secondary Organic Aerosol. *Nature* **2014**, *506* (7489), 476−479.

(13) Yan, C.; Nie, W.; Vogel, A. L.; Dada, L.; Lehtipalo, K.; Stolzenburg, D.; Wagner, R.; Rissanen, M. P.; Xiao, M.; Ahonen, L.et al. Size-Dependent Influence of NOx on the Growth Rates of Organic Aerosol Particles. *Sci. Adv.* **2020**, *6* (22), eaay4945.

(14) Rissanen, M. P.; Kurtén, T.; Sipilä, M.; Thornton, J. A.; Kangasluoma, J.; Sarnela, N.; Junninen, H.; Jørgensen, S.; Schallhart, S.; Kajos, M. K.; et al. The Formation of Highly Oxidized Multifunctional Products in the Ozonolysis of Cyclohexene. *J. Am. Chem. Soc.* **2014**, *136* (44), 15596−15606.

(15) Donahue, N. M.; Henry, K. M.; Mentel, T. F.; Kiendler-Scharr, A.; Spindler, C.; Bohn, B.; Brauers, T.; Dorn, H. P.; Fuchs, H.; Tillmann, R.; Wahner, A.; Saathoff, H.; Naumann, K.-H. H. K. H.; Möhler, O.; Leisner, T.; Müller, L.; Reinnig, M.-C. C. M. C.; Hoffmann, T.; Salo, K.; Hallquist, M.; Frosch, M.; Bilde, M.; Tritscher, T.; Barmet, P.; Praplan, A. P.; DeCarlo, P. F.; Dommen, J.; Prévôt, A. S. H.; Baltensperger, U. Aging of Biogenic Secondary Organic Aerosol via Gas-Phase OH Radical Reactions. *Proc. Natl. Acad. Sci. U. S. A.* **2012**, *109* (34), 13503−13508.

(16) Schobesberger, S.; Junninen, H.; Bianchi, F.; Lönn, G.; Ehn, M.; Lehtipalo, K.; Dommen, J.; Ehrhart, S.; Ortega, I. K.; Franchin, A.; et al. Molecular Understanding of Atmospheric Particle Formation from Sulfuric Acid and Large Oxidized Organic Molecules. *Proc. Natl. Acad. Sci. U. S. A.* **2013**, *110* (43), 17223−17228.

(17) Koppmann, R. *Volatile Organic Compounds in the Atmosphere*; Wiley Online Library, 2007.

(18) Cabrera-Perez, D.; Taraborrelli, D.; Sander, R.; Pozzer, A. Global Atmospheric Budget of Simple Monocyclic Aromatic Compounds. *Atmos. Chem. Phys.* **2016**, *16* (11), 6931−6947.

(19) Shah, S. D.; Ogunyoku, T. A.; Miller, J. W.; Cocker, D. R. On-Road Emission Rates of PAH and n-Alkane Compounds from Heavy-Duty Diesel Vehicles. *Environ. Sci. Technol.* **2005**, *39* (14), 5276−5284.

(20) Conde, F. J.; Ayala, J. H.; Afonso, A. M.; González, V. Emissions of Polycyclic Aromatic Hydrocarbons from Combustion of Agricultural and Sylvicultural Debris. *Atmos. Environ.* **2005**, *39* (35), 6654−6663.

https://dx.doi.org/10.1021/acs.est.0c02100
Environ. Sci. Technol. XXXX, XXX, XXX−XXX

(21) McDonald, J. D.; Zielinska, B.; Fujita, E. M.; Sagebiel, J. C.; Chow, J. C.; Watson, J. G. Emissions from Charbroiling and Grilling of Chicken and Beef. *J. Air Waste Manage. Assoc.* **2003**, *53* (2), 185−194.
(22) Bloss, C.; Wagner, V.; Jenkin, M. E.; Volkamer, R.; Bloss, W. J.; Lee, J. D.; Heard, D. E.; Wirtz, K.; Martin-Reviejo, M.; Rea, G.; Wenger, J. C.; Pilling, M. J. Development of a Detailed Chemical Mechanism (MCMv3.1) for the Atmospheric Oxidation of Aromatic Hydrocarbons. *Atmos. Chem. Phys.* **2005**, *5* (3), 641−664.
(23) Offenberg, J. H.; Lewis, C. W.; Lewandowski, M.; Jaoui, M.; Kleindienst, T. E.; Edney, E. O. Contributions of Toluene and α-Pinene to SOA Formed in an Irradiated Toluene/α-Pinene/NOx/Air Mixture: Comparison of Results Using 14C Content and SOA Organic Tracer Methods. *Environ. Sci. Technol.* **2007**, *41* (11), 3972−3976.
(24) Odum, J. R.; Jungkamp, T. P. W. W.; Griffin, R. J.; Flagan, R. C.; Seinfeld, J. H. The Atmospheric Aerosol-Forming Potential of Whole Gasoline Vapor. *Science (Washington, DC, U. S.)* **1997**, *276* (5309), 96−99.
(25) Forstner, H. J. L.; Flagan, R. C.; Seinfeld, J. H. Secondary Organic Aerosol from the Photooxidation of Aromatic Hydrocarbons: Molecular Composition. *Environ. Sci. Technol.* **1997**, *31* (5), 1345−1358.
(26) Molteni, U.; Bianchi, F.; Klein, F.; El Haddad, I.; Frege, C.; Rossi, M. J.; Dommen, J.; Baltensperger, U. Formation of Highly Oxygenated Organic Molecules from Aromatic Compounds. *Atmos. Chem. Phys.* **2018**, *18*, 1909−1921.
(27) Garmash, O.; Rissanen, M. P.; Pullinen, I.; Schmitt, S.; Kausiala, O.; Tillmann, R.; Zhao, D.; Percival, C.; Bannan, T. J.; Priestley, M.; Hallquist, A. M.; Kleist, E.; Kiendler-Scharr, A.; Hallquist, M.; Berndt, T.; McFiggans, G.; Wildt, J.; Mentel, T. F.; Ehn, M. Multi-Generation OH Oxidation as a Source for Highly Oxygenated Organic Molecules from Aromatics. *Atmos. Chem. Phys.* **2020**, *20*, 515−537.
(28) Dias, A.; Ehrhart, S.; Vogel, A.; Mathot, S.; Onnela, A.; Almeida, J.; Kirkby, J.; Williamson, C.; Mumford, S. Temperature Uniformity in the CERN CLOUD Chamber. *Atmos. Meas. Tech.* **2017**, *10*, 5075−5088.
(29) Bertram, T. H.; Kimmel, J. R.; Crisp, T. A.; Ryder, O. S.; Yatavelli, R. L. N.; Thornton, J. A.; Cubison, M. J.; Gonin, M.; Worsnop, D. R. A Field-Deployable, Chemical Ionization Time-of-Flight Mass Spectrometer. *Atmos. Meas. Tech.* **2011**, *4*, 1471−1479.
(30) Lopez-Hilfiker, F. D.; Mohr, C.; Ehn, M.; Rubach, F.; Kleist, E.; Wildt, J.; Mentel, T. F.; Lutz, A.; Hallquist, M.; Worsnop, D.; Thornton, J. A. A Novel Method for Online Analysis of Gas and Particle Composition: Description and Evaluation of a Filter Inlet for Gases and AEROsols (FIGAERO). *Atmos. Meas. Tech.* **2014**, *7* (4), 983−1001.
(31) Junninen, H.; Ehn, M.; Petaja, T.; Luosujarvi, L.; Kotiaho, T.; Kostiainen, R.; Rohner, U.; Gonin, M.; Fuhrer, K.; Kulmala, M.; et al. A High-Resolution Mass Spectrometer to Measure Atmospheric Ion Composition. *Atmos. Meas. Tech.* **2010**, *3* (4), 1039−1053.
(32) Kurten, A.; Jokinen, T.; Simon, M.; Sipila, M.; Sarnela, N.; Junninen, H.; Adamov, A.; Almeida, J.; Amorim, A.; Bianchi, F.; et al. Neutral Molecular Cluster Formation of Sulfuric Acid-Dimethylamine Observed in Real Time under Atmospheric Conditions. *Proc. Natl. Acad. Sci. U. S. A.* **2014**, *111* (42), 15019−15024.
(33) Stark, H.; Yatavelli, R. L. N.; Thompson, S. L.; Kang, H.; Krechmer, J. E.; Kimmel, J. R.; Palm, B. B.; Hu, W. W.; Hayes, P. L.; Day, D. A.; Campuzano-Jost, P.; Canagaratna, M. R.; Jayne, J. T.; Worsnop, D. R.; Jimenez, J. L. Impact of Thermal Decomposition on Thermal Desorption Instruments: Advantage of Thermogram Analysis for Quantifying Volatility Distributions of Organic Species. *Environ. Sci. Technol.* **2017**, *51*, 8491−8500.
(34) Wang, M. Y.; Yao, L.; Zheng, J.; Wang, X. K.; Chen, J. M.; Yang, X.; Worsnop, D. R.; Donahue, N. M.; Wang, L. Reactions of Atmospheric Particulate Stabilized Criegee Intermediates Lead to High-Molecular-Weight Aerosol Components. *Environ. Sci. Technol.* **2016**, *50*, 5702−5710.
(35) Donahue, N. M.; Epstein, S. A.; Pandis, S. N.; Robinson, A. L. A Two-Dimensional Volatility Basis Set: 1. Organic-Aerosol Mixing Thermodynamics. *Atmos. Chem. Phys.* **2011**, *11* (7), 3303−3318.
(36) Schervish, M.; Donahue, N. M. Peroxy Radical Chemistry and the Volatility Basis Set. *Atmos. Chem. Phys.* **2020**, *20*, 1183−1199.
(37) Bianchi, F.; Kurtén, T.; Riva, M.; Mohr, C.; Rissanen, M. P.; Roldin, P.; Berndt, T.; Crounse, J. D.; Wennberg, P. O.; Mentel, T. F.; Wildt, J.; Junninen, H.; Jokinen, T.; Kulmala, M.; Worsnop, D. R.; Thornton, J. A.; Donahue, N.; Kjaergaard, H. G.; Ehn, M. Highly Oxygenated Organic Molecules (HOM) from Gas-Phase Autoxidation Involving Peroxy Radicals: A Key Contributor to Atmospheric Aerosol. *Chem. Rev.* **2019**, *119* (6), 3472−3509.
(38) Emanuelsson, E. U.; Hallquist, M.; Kristensen, K.; Glasius, M.; Bohn, B.; Fuchs, H.; Kammer, B.; Kiendler-Scharr, A.; Nehr, S.; Rubach, F.; Tillmann, R.; Wahner, A.; Wu, H.-C. C.; Mentel, T. F. Formation of Anthropogenic Secondary Organic Aerosol (SOA) and Its Influence on Biogenic SOA Properties. *Atmos. Chem. Phys.* **2013**, *13* (5), 2837−2855.
(39) Pankow, J. F.; Asher, W. E. SIMPOL.1: A Simple Group Contribution Method for Predicting Vapor Pressures and Enthalpies of Vaporization of Multifunctional Organic Compounds. *Atmos. Chem. Phys.* **2008**, *8* (10), 2773−2796.
(40) Bilde, M.; Barsanti, K.; Booth, M.; Cappa, C. D.; Donahue, N. M.; Emanuelsson, E. U.; McFiggans, G.; Krieger, U. K.; Marcolli, C.; Topping, D.; Ziemann, P.; Barley, M.; Clegg, S.; Dennis-Smither, B.; Hallquist, M.; Hallquist, Å. M.; Khlystov, A.; Kulmala, M.; Mogensen, D.; Percival, C. J.; Pope, F.; Reid, J. P.; Ribeiro da Silva, M. A. V; Rosenoern, T.; Salo, K.; Soonsin, V. P.; Yli-Juuti, T.; Prisle, N. L.; Pagels, J.; Rarey, J.; Zardini, A. A.; Riipinen, I. Saturation Vapor Pressures and Transition Enthalpies of Low-Volatility Organic Molecules of Atmospheric Relevance: From Dicarboxylic Acids to Complex Mixtures. *Chem. Rev.* **2015**, *115* (10), 4115−4156.
(41) Wu, R. R.; Pan, S. S.; Li, Y.; Wang, L. M. Atmospheric Oxidation Mechanism of Toluene. *J. Phys. Chem. A* **2014**, *118* (25), 4533−4547.
(42) Wang, S. N.; Wu, R. R.; Berndt, T.; Ehn, M.; Wang, L. M. Formation of Highly Oxidized Radicals and Multifunctional Products from the Atmospheric Oxidation of Alkylbenzenes. *Environ. Sci. Technol.* **2017**, *51*, 8442−8449.
(43) Volkamer, R.; Platt, U.; Wirtz, K. Primary and Secondary Glyoxal Formation from Aromatics: Experimental Evidence for the Bicycloalkyl - Radical Pathway from Benzene, Toluene, and p-Xylene. *J. Phys. Chem. A* **2001**, *105* (33), 7865−7874.
(44) Ji, Y. M.; Zhao, J.; Terazono, H.; Misawa, K.; Levitt, N. P.; Li, Y. X.; Lin, Y.; Peng, J. F.; Wang, Y.; Duan, L.; Pan, B. W.; Zhang, F.; Feng, X. D.; An, T. C.; Marrero-Ortiz, W.; Secrest, J.; Zhang, A. L.; Shibuya, K.; Molina, M. J.; Zhang, R. Y. Reassessing the Atmospheric Oxidation Mechanism of Toluene. *Proc. Natl. Acad. Sci. U. S. A.* **2017**, *114*, 8169−8174.
(45) Klotz, B.; Sørensen, S.; Barnes, I.; Becker, K. H.; Etzkorn, T.; Volkamer, R.; Platt, U.; Wirtz, K.; Martin-Reviejo, M. Atmospheric Oxidation of Toluene in a Large-Volume Outdoor Photoreactor: In Situ Determination of Ring-Retaining Product Yields. *J. Phys. Chem. A* **1998**, *102* (50), 10289−10299.
(46) Olariu, R. I.; Klotz, B.; Barnes, I.; Becker, K. H.; Mocanu, R. FT-IR Study of the Ring-Retaining Products from the Reaction of OH Radicals with Phenol, o-, m-, and p-Cresol. *Atmos. Environ.* **2002**, *36* (22), 3685−3697.
(47) Schwantes, R. H.; Schilling, K. A.; McVay, R. C.; Lignell, H.; Coggon, M. M.; Zhang, X.; Wennberg, P. O.; Seinfeld, J. H. Formation of Highly Oxygenated Low-Volatility Products from Cresol Oxidation. *Atmos. Chem. Phys.* **2017**, *17* (5), 3453−3474.
(48) Iyer, S.; Lopez-Hilfiker, F.; Lee, B. H.; Thornton, J. A.; Kurtén, T.; Kurten, T. Modeling the Detection of Organic and Inorganic Compounds Using Iodide-Based Chemical Ionization. *J. Phys. Chem. A* **2016**, *120* (4), 576−587.
(49) Zhao, B.; Wang, S.; Donahue, N. M.; Chuang, W.; Hildebrandt Ruiz, L.; Ng, N. L.; Wang, Y.; Hao, J. Evaluation of One-Dimensional and Two-Dimensional Volatility Basis Sets in Simulating the Aging of Secondary Organic Aerosol with Smog-Chamber Experiments. *Environ. Sci. Technol.* **2015**, *49* (4), 2245−2254.
(50) Zhao, B.; Wang, S.; Donahue, N. M.; Jathar, S. H.; Huang, X.; Wu, W.; Hao, J.; Robinson, A. L. Quantifying the Effect of Organic

https://dx.doi.org/10.1021/acs.est.0c02100
Environ. Sci. Technol. XXXX, XXX, XXX−XXX

Aerosol Aging and Intermediate-Volatility Emissions on Regional-Scale Aerosol Pollution in China. *Sci. Rep.* **2016**, *6* (June), 28815.
(51) Donahue, N. M.; Chuang, W.; Epstein, S. A.; Kroll, J. H.; Worsnop, D. R.; Robinson, A. L.; Adams, P. J.; Pandis, S. N. Why Do Organic Aerosols Exist? Understanding Aerosol Lifetimes Using the Two-Dimensional Volatility Basis Set. *Environ. Chem.* **2013**, *10*, 151−157.
(52) Riccobono, F.; Schobesberger, S.; Scott, C. E.; Dommen, J.; Ortega, I. K.; Rondo, L.; Almeida, J.; Amorim, A.; Bianchi, F.; Breitenlechner, M.; et al. Oxidation Products of Biogenic Emissions Contribute to Nucleation of Atmospheric Particles. *Science (Washington, DC, U. S.)* **2014**, *344* (6185), 717−721.
(53) Nieminen, T.; Lehtinen, K. E. J.; Kulmala, M. Sub-10 Nm Particle Growth by Vapor Condensation − Effects of Vapor Molecule Size and Particle Thermal Speed. *Atmos. Chem. Phys.* **2010**, *10* (20), 9773−9779.

https://dx.doi.org/10.1021/acs.est.0c02100
Environ. Sci. Technol. XXXX, XXX, XXX−XXX